Proceedings of ASME 2013 International Mechanical Engineering Congress & Exposition
IMECE2013
November 15-21, 2013, San Diego, USA

IMECE2013-62036

AN OPERATIONALLY OPTIMIZED SEVEN LINK BIPED ROBOT MOVING ON SLOPES

Peiman Naseradinmousavi
Assistant Professor
Department of Mechanical and Applied Engineering
Indiana State University
Terre Haute, IN 47809
Email: peiman.naseradinmousavi@villanova.edu

ABSTRACT

In this paper, we discuss operational optimization of a seven link biped robot using the well-known "Simulated Annealing" algorithm. Some critical parameters affecting the robot gait pattern are selected to be optimized reducing the total energy used. Nonlinear modeling process we published elsewhere is shown here for completeness. The trajectories of both the hip and ankle joints are used to plan the robot gait on slopes and undoubtedly those parameters would be the target ones for the optimization process. The results we obtained reveal considerable amounts of the energy saved for both the ascending and descending surfaces while keeping the robot stable. The stability criterion we utilized for both the modeling and then optimization is "Zero Moment Point". A comparative study of human evolutionary gait and the operationally optimized robot is also presented.

INTRODUCTION

Requirements for smart mechanisms are developing for advanced industrial and military demands. The latter particularly has been investigated widely and novel advancements have been offered by researchers [1]. Biped robots have received much attention recently even for utilizing in battle fields. On the other hand, the sensitive situations need to be considered carefully from the point of view of both the stability and optimality concerns.

Optimality becomes significant where tens of the robots are supposed to operate in a network (mission) and consequently a remarkable amount of energy is expected to be used. From another aspect, a biped walks like we do for more than million times and hence an optimized gait fashion is needed to be developed to save energy. Two optimization schemes typically are used to minimize the energy used in the system. The first is so-called "Optimal Design" dealing with some geometrical and inertial parameters as target ones for the optimization process. The second known as "Optimal Operation" utilizes some operational parameters for minimizing the cost function.

We, on the other hand, are looking for any particular fashion of the robot gait to minimize the energy used by the actuators while keeping it stable. The stability criterion has been added to the literature by Vukobratovic *et al.* [2]. Taking care of the robot stability undoubtedly would apply constraints for the optimization process and we hence are not allowed to select the parameters at will. Subsequently, a constrained optimization scheme needs to be developed by defining lower and upper bounds for the target parameters.

Some efforts [3]- [9] have been on the optimization of bipeds but different from the work we carried out here. Quasi optimal gait of a biped robot with a rolling knee kinematic has been researched by Hobon *et al.* [10]. Their simulation results showed that the energy consumption of the new biped with *rolling knee* contact is less than that of the robot with revolute joint knees. Yoon *et al.* [11] adopted the genetic algorithm for minimizing energy consumption. They proposed a new parallel mechanism of biped robots, each of its legs is composed of two 3 - DOF parallel platforms linked serially. Piao *et al.* [12] introduced two BP

Copyright © 2013 by ASME

networks into train the walking trajectory of robot and developed the optimal trajectory by the new evolutionary approach based on particle swarm optimization.

We represent the inverse kinematic and dynamic approaches reported elsewhere to derive the driving torques with the aid of the Lagrangian method. The optimization process we developed here is for "single support phase" where the robot is only supported by one leg. The "double support phase" presents limited motions and no sense to optimize it operationally by scarifying the speed of calculations. Then the problem setup is shown by explaining how the simulated annealing works and what are the constraints. A comparative discussion for human evolutionary gait and the operationally optimized robot is carried out in the course of this work.

MATHEMATICAL MODELING

We developed a comprehensive mathematical model [13,14] using inverse kinematic and dynamic approaches. Fig. 1 shows a schematic model of the robot. Trajectories for the hip and ankle joints are as follows.

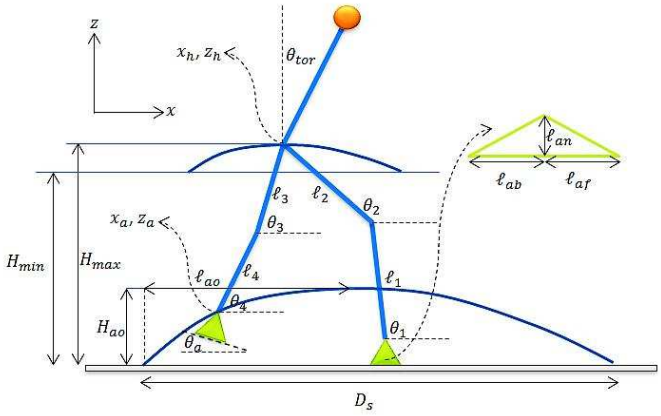

FIGURE 1. The robot configuration

Ankle joint:

$$\theta_a = \begin{cases} -q_{gs} + \lambda & t = kT_c \\ -q_b + \lambda & t = kT_c + T_d \\ q_f + \lambda & t = (k+1)T_c \\ q_{gf} + \lambda & t = (k+1)T_c + T_d \end{cases} \quad (1)$$

$$x_a = \begin{cases} kD_s\cos\lambda - \ell_{an}\sin\lambda & t = kT_c \\ (kD_s + \ell_{af})\cos\lambda + \ldots & t = kT_c + T_d \\ \ell_{an}\sin(q_b - \lambda) - \ell_{af}\cos(q_b - \lambda) & \\ (kD_s + \ell_{ao})\cos\lambda & t = kT_c + T_m \\ ((k+2)D_s - \ell_{ab})\cos\lambda - \ldots & t = (k+1)T_c \\ \ell_{an}\sin(q_f + \lambda) + \ell_{ab}\cos(q_f + \lambda) & \\ (k+2)D_s\cos\lambda - \ell_{an}\sin\lambda & t = (k+1)T_c \\ & +T_d \end{cases} \quad (2)$$

$$z_a = \begin{cases} kD_s\sin\lambda + \ell_{an}\cos\lambda & t = kT_c \\ (kD_s + \ell_{af})\sin\lambda + \ldots & t = kT_c + T_d \\ \ell_{an}\cos(q_b - \lambda) + \ell_{af}\sin(q_b - \lambda) & \\ (kD_s + \ell_{ao})\sin\lambda + H_{ao}\cos\lambda & t = kT_c + T_m \\ ((k+2)D_s - \ell_{ab})\sin\lambda + \ldots & t = (k+1)T_c \\ \ell_{an}\sin(q_f + \lambda) + \ldots & \\ \ell_{ab}\cos(\pi/2 - (q_f + \lambda)) & \\ (k+2)D_s\sin\lambda + \ell_{an}\cos\lambda & t = (k+1)T_c \\ & +T_d \end{cases} \quad (3)$$

Similar to the human walking process we apply the following boundary conditions.

$$\begin{cases} \dot{\theta}_a(kT_c) = 0 \\ \dot{\theta}_a((k+1)T_c + T_d) = 0 \end{cases} \quad (4)$$

$$\begin{cases} \dot{x}_a(kT_c) = 0 \\ \dot{x}_a((k+1)T_c + T_d) = 0 \end{cases} \quad (5)$$

$$\begin{cases} \dot{z}_a(kT_c) = 0 \\ \dot{z}_a((k+1)T_c + T_d) = 0 \end{cases} \quad (6)$$

Hip joint:

$$x_h = \begin{cases} (kD_s + x_{ed})\cos\lambda & t = kT_c \\ ((k+1)D_s - x_{sd})\cos\lambda & t = kT_c + T_d \\ ((k+1)D_s + x_{ed})\cos\lambda & t = (k+1)T_c \end{cases} \quad (7)$$

Copyright © 2013 by ASME

$$z_h = \begin{cases} H_{min}\cos\lambda + (kD_s + x_{ed})\sin\lambda & t = kT_c \\ H_{max}\cos\lambda + (kD_s + x_{sd})\sin\lambda & t = kT_c + \\ & 0.5(T_c - T_d) \\ ((k+1)D_s + x_{ed})\sin\lambda + & t = (k+1)T_c \\ H_{min}\cos\lambda & \end{cases} \quad (8)$$

where, T_c: total traveling time, including single and double support phases, T_d: double support phase time, which it is regarded as 20% of T_c, T_m: the time which ankle joint has reached maximum height during walking cycle, k: step number, H_{ao}: ankle joint maximum height, ℓ_{ao}: the horizontal traveled distance between ankle joint and start point when the ankle joint has reached its maximum height, D_s:step length, q_b, q_f: foot lift angle and contact angle with the level ground, q_{gs}, q_{gf}: the ground initial terrain angles, λ: surface slope, H_{min}, H_{max}: the hip minimum and maximum heights measured from the fixed coordinate system, x_{ed}, x_{sd}: the distance between the hip and fixed coordinate system which is supposed to be on the support leg, will be denoted for the instants of the beginning and the end points of the double support phase.

The breakpoints given enable us to fit the following curves to generate the robot path.

$$\begin{cases} \theta_a(t) \\ x_a(t) \\ z_a(t) \\ x_h(t) \\ z_h(t) \end{cases} = \begin{cases} \sum_{i=1}^{6} \alpha_i t^i \\ \sum_{i=1}^{7} \beta_i t^i \\ \sum_{i=1}^{7} \gamma_i t^i \\ \sum_{i=1}^{5} \eta_i t^i \\ \sum_{i=1}^{5} \omega_i t^i \end{cases} \quad (9)$$

The angles of the links hence are obtained by solving the following nonlinear equations:

$$\ell_1\cos(\pi-\theta_1) + \ell_2\cos(\pi-\theta_2) = x_{a,sup} - x_h \quad (10)$$
$$\ell_3\cos(\theta_3) + \ell_4\cos(\theta_4) = x_h - x_{a,swg} \quad (11)$$
$$\ell_1\sin(\pi-\theta_1) + \ell_2\sin(\pi-\theta_2) = z_h - z_{a,sup} \quad (12)$$
$$\ell_3\sin(\theta_3) + \ell_4\sin(\theta_4) = z_h - z_{a,swg} \quad (13)$$

where, *sup* and *swg* stand for the support and swing legs, respectively. Angular velocities and accelerations are also known by having the links' angles. The next step is to utilize the Lagrangian equation to derive the driving torques needed for the robot motion based on the paths given, obviously for the single support phase.

$$\frac{d}{dt}\left(\frac{\partial Ł}{\partial \dot{q}_k}\right) - \frac{\partial Ł}{\partial q_k} = \tau_i \quad (14)$$

where $Ł = \sum_{i=1}^{n} T_i - \sum_{i=1}^{n} V_i$. T_i and V_i stand for the kinetic and potential energies of each link, respectively.

$$q = [\theta_1, \theta_2, \theta_3, \theta_4, \theta_a, \theta_{tor}] \quad (15)$$
$$T_i = 0.5(m_i{}^i v_{ci}^2 + {}^i I_i \dot{\theta}_i^2) \quad (16)$$
$$V_i = m_i g z_{ci} \quad (17)$$

where, q is a lumped set of the angles, V_{ci} is the velocity of mass center of link i, and θ_{tor} indicates the torso deflection from the vertical axis (z). The Lagrangian equation leads to:

$$\tau_i = H(q)\ddot{q} + C(q,\dot{q})\dot{q} + G(q) \quad (18)$$

where H, C, and G are mass inertia, coriolis, and gravitational matrices, respectively, yielding the following equation:

$$\begin{bmatrix} h_{11} & h_{12} & h_{13} & h_{14} & h_{15} & h_{16} \\ h_{21} & h_{22} & h_{23} & h_{24} & h_{25} & h_{26} \\ h_{31} & h_{32} & h_{33} & h_{34} & h_{35} & h_{36} \\ h_{41} & h_{42} & h_{43} & h_{44} & h_{45} & h_{46} \\ h_{51} & h_{52} & h_{53} & h_{54} & h_{55} & h_{56} \\ h_{61} & h_{62} & h_{63} & h_{64} & h_{65} & h_{66} \end{bmatrix} \begin{bmatrix} \ddot{\theta}_1 \\ \ddot{\theta}_2 \\ \ddot{\theta}_3 \\ \ddot{\theta}_4 \\ \ddot{\theta}_a \\ \ddot{\theta}_{tor} \end{bmatrix} \quad (19)$$

$$+ \begin{bmatrix} c_{11} & c_{12} & c_{13} & c_{14} & c_{15} & c_{16} \\ c_{21} & c_{22} & c_{23} & c_{24} & c_{25} & c_{26} \\ c_{31} & c_{32} & c_{33} & c_{34} & c_{35} & c_{36} \\ c_{41} & c_{42} & c_{43} & c_{44} & c_{45} & c_{46} \\ c_{51} & c_{52} & c_{53} & c_{54} & c_{55} & c_{56} \\ c_{61} & c_{62} & c_{63} & c_{64} & c_{65} & c_{66} \end{bmatrix} \begin{bmatrix} \dot{\theta}_1 \\ \dot{\theta}_2 \\ \dot{\theta}_3 \\ \dot{\theta}_4 \\ \dot{\theta}_a \\ \dot{\theta}_{tor} \end{bmatrix} \quad (20)$$

$$+ \begin{bmatrix} G_1 \\ G_2 \\ G_3 \\ G_4 \\ G_a \\ G_{tor} \end{bmatrix} = \begin{bmatrix} \tau_1 \\ \tau_2 \\ \tau_3 \\ \tau_4 \\ \tau_a \\ \tau_{tor} \end{bmatrix} \quad (21)$$

The components of the matrices [13] shown above yield the torques needed for the paths planned. For an example h_{11} is shown here by numbering the links as support shank=1, support tight=2, swing shank=3, swing tight=4, swing foot=5, and torso=6.

Copyright © 2013 by ASME

TABLE 1. The geometrical and inertial parameters

$\ell_{i=1-4,tor}$	0.3 m	D_s	0.5 m
ℓ_{ab}	0.1 m	ℓ_{an}	0.1 m
ℓ_{af}	0.13 m	$x_{ed} = x_{sd}$	0.23 m
ℓ_{ao}	0.25 m	H_{ao}	0.15 m
T_c	0.9 s	T_d	0.18 s
T_m	0.4 s	$q_b = q_f$	0.2 rad
m_{sh}	5.7 kg	m_{ti}	10 kg
m_{tor}	43 kg	m_{foot}	3.3 kg
I_{sh}	0.08 kg-m^2	I_{ti}	0.02 kg-m^2
I_{tor}	1.4 kg-m^2	I_{foot}	0.01 kg-m^2

$$
\begin{aligned}
h_{11} &= [m_1(\ell_{c1}^2 + \ell_{c1}\ell_e\cos(\theta_1-\phi))] + [m_2(\ell_1^2+\ell_{c2}^2 \\
&+ \ell_1\ell_e\cos(\theta_1-\phi) + \ell_{c2}\ell_e\cos(\theta_2-\phi) + 2\ell_1\ell_{c2} \\
&\quad \cos(\theta_2-\theta_1))] + [m_3(\ell_1^2+\ell_2^2+\ell_{c3}^2 \\
&+ \ell_1\ell_e\cos(\theta_1-\phi) + \ell_2\ell_e\cos(\theta_2-\phi) - \ell_{c3}\ell_e\cos(-\theta_3+\phi) \\
&+ 2\ell_1\ell_2\cos(\theta_2-\theta_1) - 2\ell_1\ell_{c3}\cos(\theta_1-\theta_3) \\
&- 2\ell_2\ell_{c3}\cos(\theta_2-\theta_3))] + [m_4(\ell_1^2+\ell_2^2+\ell_3^2 \\
&+ \ell_{c4}^2 + \ell_1\ell_e\cos(\theta_1-\phi) + \ell_2\ell_e\cos(\theta_2-\phi) \\
&- \ell_3\ell_e\cos(\theta_3-\phi) - \ell_{c4}\ell_e\cos(-\theta_4+\phi) \\
&+ 2\ell_1\ell_2\cos(\theta_2-\theta_1) - 2\ell_1\ell_3\cos(\theta_3-\theta_1) \\
&- 2\ell_1\ell_{c4}\cos(\theta_1-\theta_4) - 2\ell_2\ell_3\cos(\theta_3-\theta_2) \\
&- 2\ell_2\ell_{c4}\cos(\theta_2-\theta_4) + 2\ell_3\ell_{c4}\cos(\theta_3-\theta_4))] \\
&+ [m_5(\ell_1^2+\ell_2^2+\ell_3^2+\ell_4^2+\ell_5^2 \\
&+ \ell_1\ell_e\cos(\theta_1-\phi) + \ell_2\ell_e\cos(\theta_2-\phi) \\
&- \ell_3\ell_e\cos(\theta_3-\phi) - \ell_4\ell_e\cos(\theta_4-\phi) \\
&- \ell_5\ell_e\cos(\phi-(\pi/2)+\theta_5-\beta) + 2\ell_1\ell_2\cos(\theta_2-\theta_1) \\
&- 2\ell_1\ell_3\cos(\theta_3-\theta_1) - 2\ell_1\ell_4\cos(\theta_4-\theta_1) \\
&- 2\ell_5\ell_1\cos(\theta_1-(\pi/2)+\theta_5-\beta) - 2\ell_2\ell_3\cos(\theta_3-\theta_2) \\
&- 2\ell_2\ell_4\cos(\theta_4-\theta_2) - 2\ell_2\ell_5\cos(\theta_2-(\pi/2)+\theta_5-\beta) \\
&+ 2\ell_3\ell_4\cos(\theta_4-\theta_3) + 2\ell_3\ell_5\cos(\theta_3-(\pi/2)+\theta_5-\beta) \\
&+ 2\ell_4\ell_5\cos(\theta_4-(\pi/2)+\theta_5-\beta))] + [m_3(\ell_1^2+\ell_2^2+\ell_{c6}^2 \\
&+ \ell_1\ell_e\cos(\theta_1-\phi) + \ell_2\ell_e\cos(\theta_2-\phi) + \ell_{c6}\ell_e\cos(-\theta_6-\phi-(\pi/2)) \\
&+ 2\ell_1\ell_2\cos(\theta_2-\theta_1) + 2\ell_1\ell_{c6}\cos(-\theta_6-\theta_1-(\pi/2)) \\
&+ 2\ell_2\ell_{c6}\cos(\theta_6+\theta_2+(\pi/2))] + I_1 + I_2 + I_3 + I_4 + I_5 + I_6
\end{aligned}
\tag{22}
$$

Given the geometrical and inertial parameters in Table 1 enable us to simulate the robot nominal gaits shown in Figs. 2(a) and 2(b), in the Sagittal plane, for the descending and ascending surfaces, respectively (with the aid of MATLAB coding).

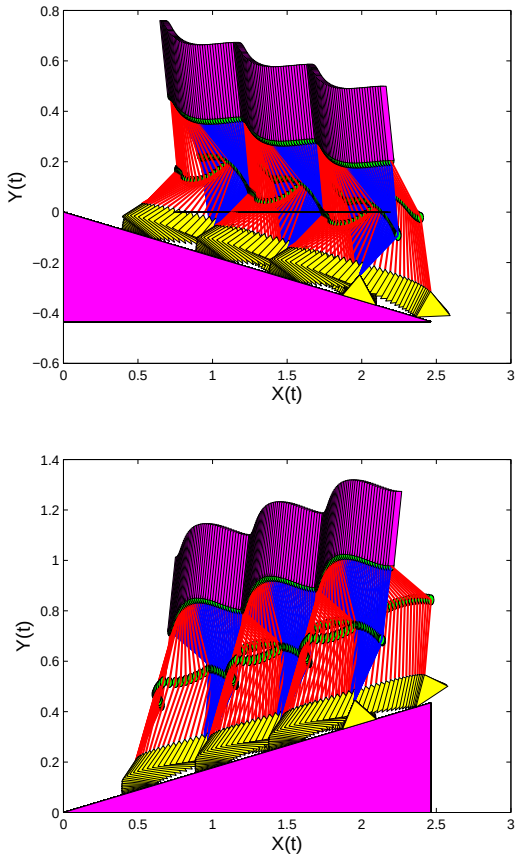

FIGURE 2. Nominal gait of the robot in the Sagittal plane: (a) $\lambda = -10^\circ$ (b) $\lambda = +10^\circ$

The nominal steps need the following total energies to be used:

$$E_{noma} = \sum_{i=1}^{6}\int_{T_d}^{T_c} \tau_i\dot{\theta}_i = 200.3885\frac{N.m.rad}{s} \tag{23}$$

$$E_{nomd} = \sum_{i=1}^{6}\int_{T_d}^{T_c} \tau_i\dot{\theta}_i = 569.6866\frac{N.m.rad}{s} \tag{24}$$

where E_{noma} and E_{nomd} stand for the nominal energies used in the ascending and descending motions, respectively. The robot, at the same time, needs to be stable and we can examine it with the aid of "Zero Moment Point" criterion. The ZMP is calculated as follows.

$$x_{zmp} = \frac{\sum_{i=1}^{n} m_i(g\cos\lambda + \ddot{z}_i)x_i - \sum_{i=1}^{n} m_i(g\sin\lambda + \ddot{x}_i)z_i - \sum_{i=1}^{n} {}^{i}I_i\dot{\theta}_i^2}{\sum_{i=1}^{n} m_i(g\cos\lambda + \ddot{z}_i)} \tag{25}$$

where $\ddot{x}_i$ and $\ddot{z}_i$ are mass center's vertical and horizontal acceleration of link i with respect to the fixed coordinate system, respec-

Copyright © 2013 by ASME

tively. The nominal paths planned satisfy the system stability

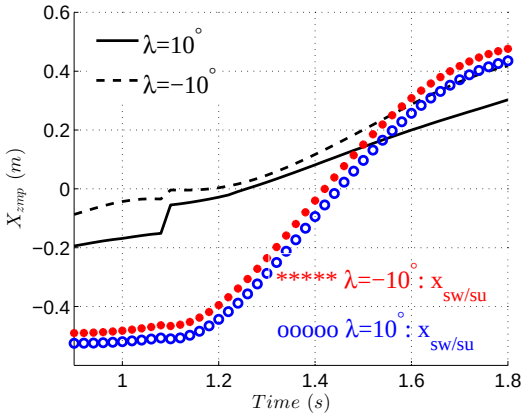

FIGURE 3. The ZMP for the nominal gaits and the swing leg positions with respect to the support ones

shown in Fig. 3 indicating X_{zmp}s move between the swing and support legs. It is straightforward to conclude that the robot is stable by comparing the ZMP's position with that of the swing leg measured from the support one (x_{sw}/x_{su}). Note that the ZMPs shown are measured from the coordinate system attached to the support leg.

Optimization

We then need to optimize the path in order to minimize the amount of energy used while keeping the robot stable. Operational optimization emerges as of the reliable solutions. The question is that how to setup the optimization scheme to avoid local minima and subsequently a time consuming process. The well-known "Simulated Annealing (SA)" algorithm as one of the global optimization tools looks suitable with respect to the problem configuration.

The name of the simulated annealing has been taken from the annealing process used in the metallurgical studies as one of the methods to relieve stress with the aid of "heat treatment". Increasing the system temperature causes higher kinetic energy for atoms and we, on the other hand, increase the system energy level. The next step is to cool the system down gradually in the ambient temperature. Doing this decreases the system energy level and gives freedoms to atoms to find the positions with minimum internal energy. The method was independently developed by Kirkpatrick *et al.* [15] and by Cerny [16]. The method is an adaptation of the Metropolis-Hastings algorithm, a Monte Carlo method generating sample states of a thermodynamic system, introduced by Rosenbluth in a paper by Metropolis *et al.* in 1953 [17].

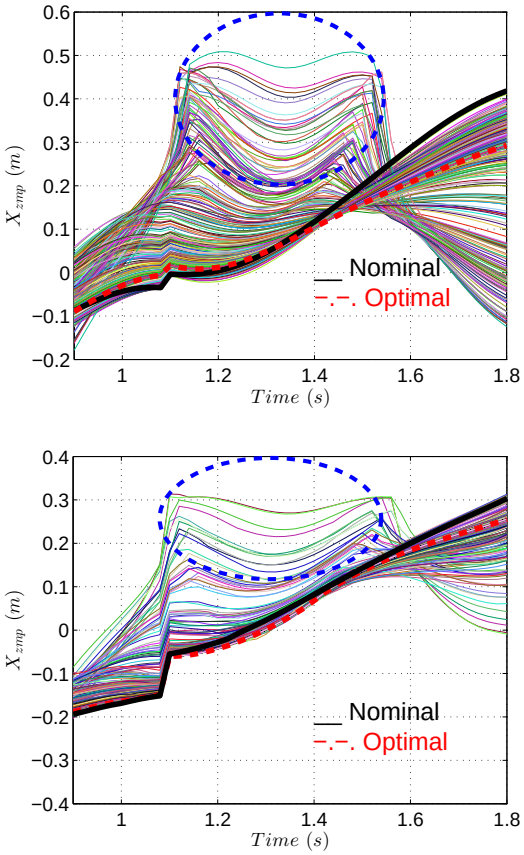

FIGURE 4. The optimized x_{zmp}: (a) $\lambda = -10°$ (b) $\lambda = +10°$

This tool helps us optimize the robot path by defining some operational parameters for both the hip and ankle joints as follows:

$$\theta = [D_s, H_{min}, H_{max}, \ell_{ao}, H_{ao}] \tag{26}$$

Note that our approach is the path planning with the aid of the breakpoints given and logically the optimization needs to be carried out on some critical breakpoints generating the paths. This method covers all search domain and yields global minima. The cost function we need to minimize is as below.

$$\min E = \min \sum_{i=1}^{6} \int_{T_d}^{T_c} \tau_i \dot{\theta}_i \tag{27}$$

Note that we are not allowed to select the parameters at will where the stability issue needs to be regarded. The stability hence applies constraints on the optimization task by defining lower and

Copyright © 2013 by ASME

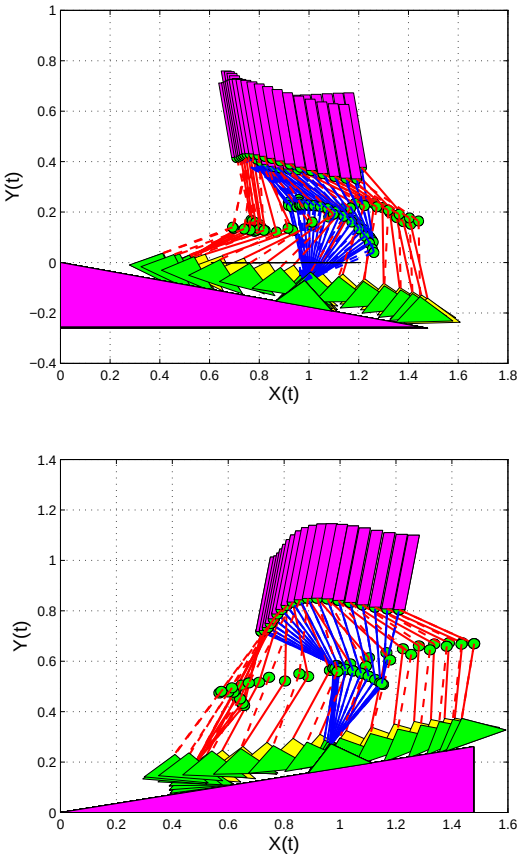

FIGURE 5. Stick Diagrams for the nominal and optimal responses: (a) $\lambda = -10^\circ$ (b) $\lambda = +10^\circ$

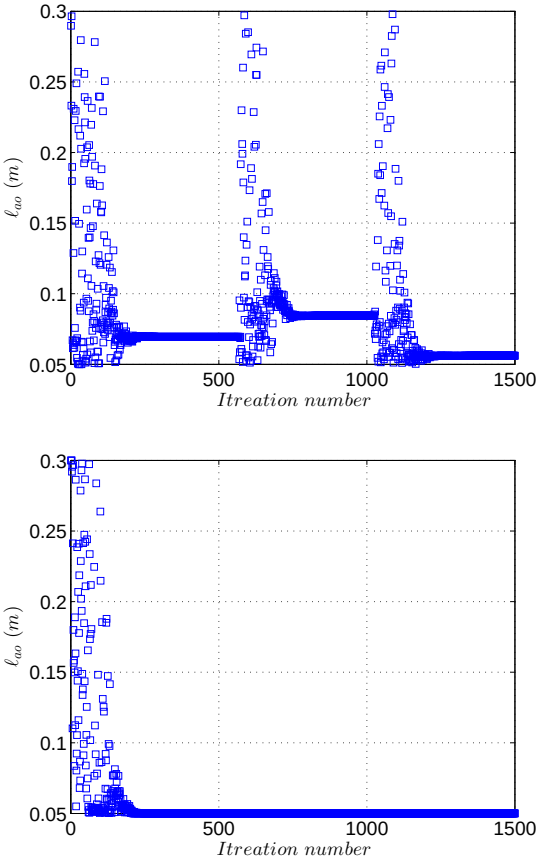

FIGURE 6. The optimized ℓ_{ao}: (a) $\lambda = -10^\circ$ (b) $\lambda = +10^\circ$

upper bounds for those parameters as the following:

$$\theta_{min} = [0.1, 0.55, 0.62, 0.05, 0.1] \quad (28)$$
$$\theta_{max} = [0.5, 0.6, 0.67, 0.3, 0.25] \quad (29)$$

Another point we have to be cautious is the initial guesses sometimes causing to be trapped in local minima. The solution is to utilize random initial guesses as below.

$$D_{s0} = D_{sl} + (D_{su} - D_{sl})\text{rand}(0,1) \quad (30)$$
$$\ell_{ao0} = \ell_{aol} + (\ell_{aou} - \ell_{aol})\text{rand}(0,1) \quad (31)$$
$$H_{min0} = H_{minl} + (H_{minu} - H_{minl})\text{rand}(0,1) \quad (32)$$
$$H_{max0} = H_{maxl} + (H_{maxu} - H_{maxl})\text{rand}(0,1) \quad (33)$$
$$H_{ao0} = H_{aol} + (H_{aou} - H_{aol})\text{rand}(0,1) \quad (34)$$

where rand(0,1) is a random number between zero and one. We developed a code in MATLAB and captured remarkable results.

DISCUSSION

Figs. 4(a) and 4(b) show a set of X_{zmp}s for both the descending and ascending surfaces, respectively, illustrating how the simulated annealing works. Using the random initial guesses the algorithm generates the paths optimized to minimize the energy used. The unstable regions stated above are shown with the aid of dashed blue circles.

Shown in Figs. 5(a) and 5(b) are stick diagrams for the robot motion using both the nominal and optimal parameters. The solid red and blue lines presenting the swing and support legs, respectively, stand for the nominal and the dashed ones for the optimal gait. The optimization for the target parameters are shown in Figs. 6-11. It is of great interest to distinguish that the robot paths optimized correspond the human evolutionary gait.

This claim is supported by Figs. 6(a) and 6(b) indicating a considerable smaller value of ℓ_{ao} than the nominal value (0.25 m). This can be translated as follows. For the human gait, the maximum height for the swing ankle happens too close to the position it leaves the ground. The optimized ℓ_{ao}s shown in Figs. 6(a) and 6(b) confirm such an *evolutionary* behavior minimizing the energy used. Logically we may also expect a smaller value

Copyright © 2013 by ASME

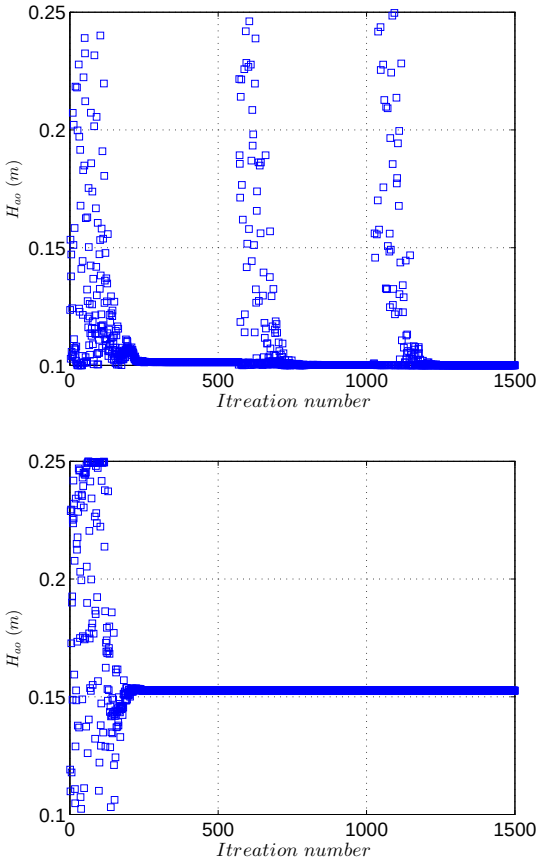

FIGURE 7. The optimized H_{ao}: (a) $\lambda = -10^\circ$ (b) $\lambda = +10^\circ$

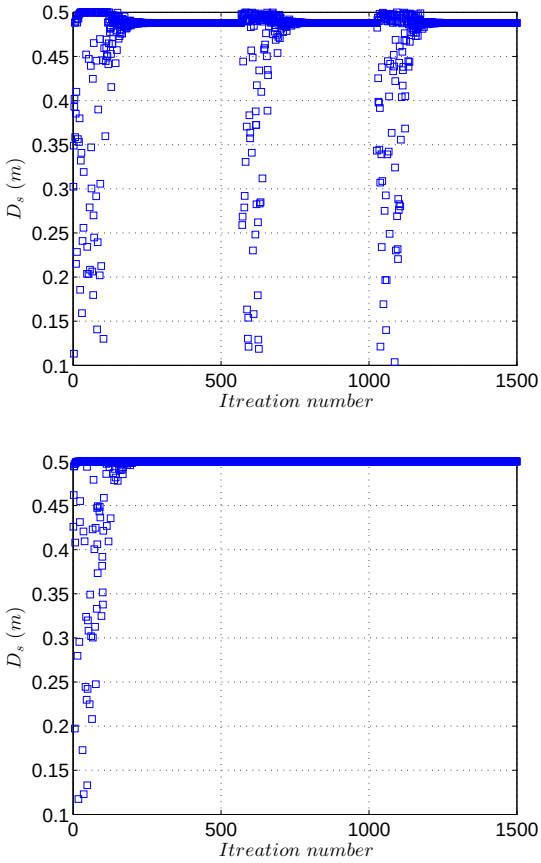

FIGURE 8. The optimized D_s: (a) $\lambda = -10^\circ$ (b) $\lambda = +10^\circ$

for the swing ankle height than its nominal value (0.16 m) which is supported by the optimization process shown in Figs. 7(a) and 7(b). Increasing the value of H_{ao} needs more energy to drive the robot and, at the same time, the stability issue becomes more critical; we may experience it physically by walking with the nominal ℓ_{ao} and H_{ao}. We, on the other hand, would need more torques to step with higher values of ℓ_{ao} and H_{ao} for a fixed D_s.

Random initial guesses can be observed for the parameters optimized trying to escape from local minima as shown in Fig. 6(a). The algorithm terminates after 1500 iterations after satisfying the tolerances defined for both the parameters and cost function; we here defined it as 10^{-12}.

Note that we fixed the time interval of the robot operation and hence the best option for the step size (D_s), similar to the human gait, is the maximum value. This is shown in Figs. 8(a) and 8(b) indicating $D_{sa} = D_{sd} \approx 0.5$ m. This seems logical in the sense that a smaller value of D_s needs more steps at that fixed time interval and clearly higher energy used.

Shown in Fig. 9(a) is the minimum hip height of $\lambda = -10^\circ$ considerably lower than that of the nominal one whereas its value for $\lambda = 10^\circ$ remains almost unchanged, as shown in Fig. 9(b). The same behavior is valid for the maximum hip height by presenting a higher value of H_{max} for the descending surface and the unchanged one for the ascending slope. These can be interpreted with the aid of the fact that the higher value of H_{max} leads to smaller ranges of $\theta_{i=1-4}$ than those of the nominal gait and hence we need to consume less energy to drive the links. This claim can be visualized in Figs. 5(a) and 5(b). Note that the human gait is similar to the robot optimized path and consequently we use minimum energy for our daily walking process.

Figs. 11(a) and 11(b) show the optimized energies revealing considerable amounts of the energy saving with respect to the nominal values particularly for the descending slope as the gravity helps the motion.

$$\Delta E_a = \left(1 - \frac{E_{opa}}{E_{noa}}\right) \approx 25\% \tag{35}$$

$$\Delta E_d = \left(1 - \frac{E_{opd}}{E_{nod}}\right) \approx 89\% \tag{36}$$

where, E_{no} and E_{op} stand for the nominal and optimal ener-

Copyright © 2013 by ASME

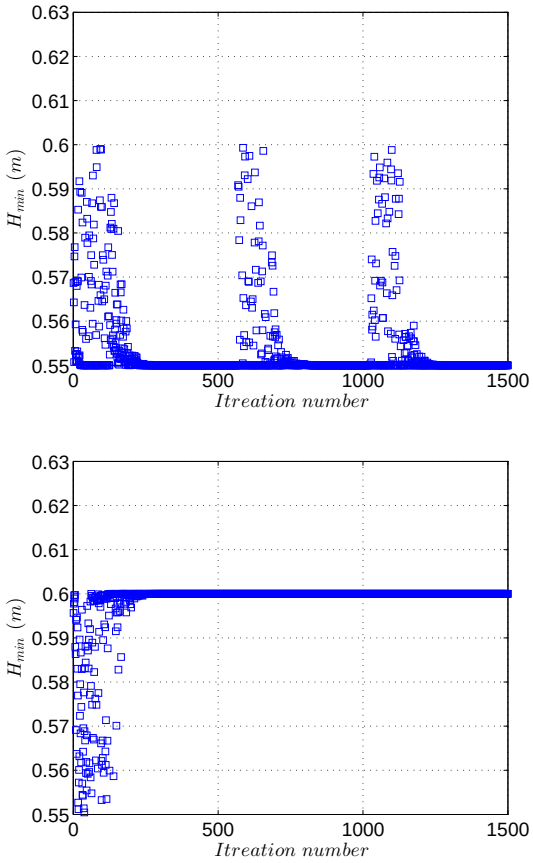

FIGURE 9. The optimized H_{min}: (a) $\lambda = -10^\circ$ (b) $\lambda = +10^\circ$

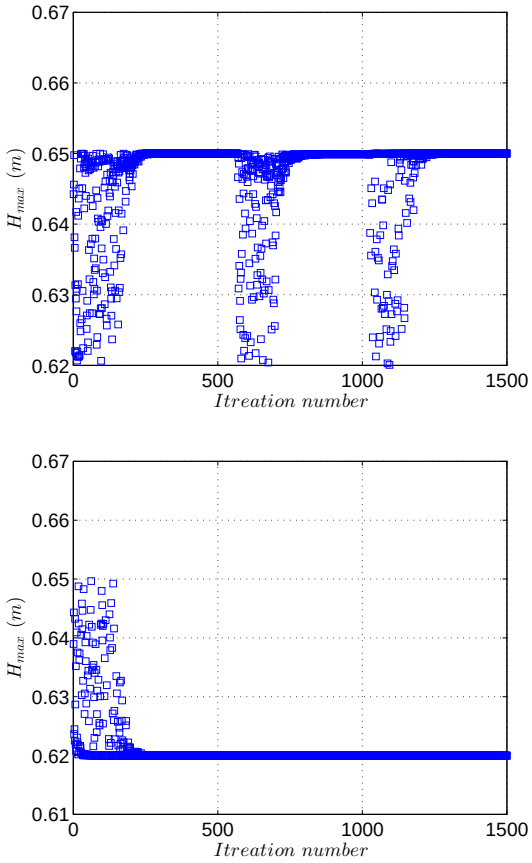

FIGURE 10. The optimized H_{max}: (a) $\lambda = -10^\circ$ (b) $\lambda = +10^\circ$

TABLE 2. The nominal and optimal parameters for $\lambda = -10^\circ$ and $\lambda = 10^\circ$

	Nominal	$\lambda = -10^\circ$	$\lambda = 10^\circ$
ℓ_{ao}	0.25 m	0.062 m	0.05 m
H_{ao}	0.16 m	0.1 m	0.15 m
H_{min}	0.6 m	0.55 m	0.6 m
H_{max}	0.62 m	0.65 m	0.62 m
D_s	0.5 m	0.5 m	0.4992 m

gies used, respectively. These remarkable amounts of the energy saved uncover the reason for the evolutionary fashion of the human gait particularly knowing that it happens millions of times in his/her life.

A list of both the nominal and optimal parameters is shown in Table 2.

CONCLUSION

In this effort we utilized the well-known simulated annealing algorithm to optimize the operation of a seven link biped robot in order to minimize the energy used. We selected both the ankle and hip joints' parameters, based on the path planning method utilized, to be optimized regarding the constraints applied by the robot stability criterion which is so-called Zero Moment Point.

The parameters optimized reveal interesting points explaining the reason of the human evolutionary gait where the maximum height of the swing ankle happens too close to the position it leaves the ground helping to consume the minimum energy. On the other hand, the smaller values of ℓ_{ao} and H_{ao} and also the higher value of H_{max} for the descending surface help reduce the links' angular velocities leading to a higher amount of the energy saved.

We captured remarkable values of the energy saving upward of 25% and 80% for the ascending and descending slopes, respectively, explaining why we need to step like the paths optimized for the robot. The next effort will be on the optimization of combined trajectory paths of the robot.

Copyright © 2013 by ASME

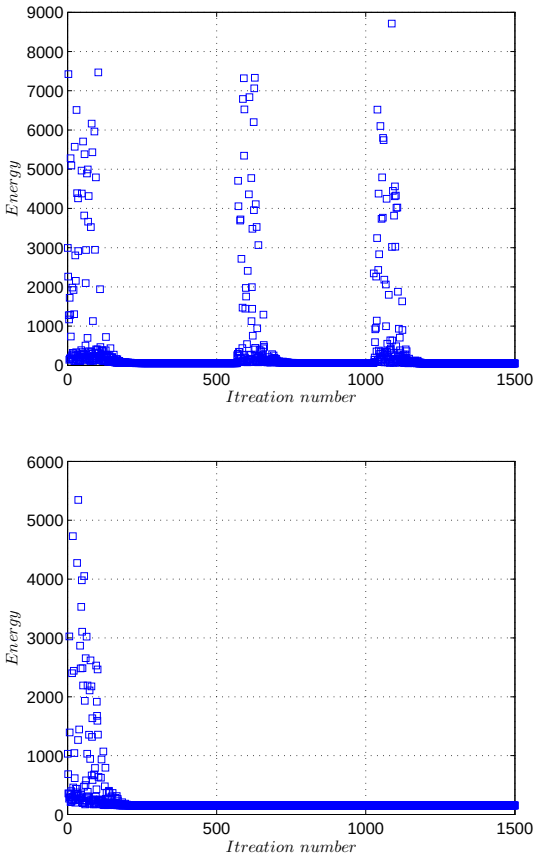

FIGURE 11. The minimized energy: (a) $\lambda = -10^{\circ}$ (b) $\lambda = +10^{\circ}$

REFERENCES

[1] http://www.bostondynamics.com/robotpetman.html.

[2] M. Vukobratovic and D. Juricic, Contribution to the synthesis of biped gait, IEEE Trans. Bio-Med. Eng. BME-16 (1) 16 (1969).

[3] F. Plestan and J. W. Grizzle, Stable walking of a 7-DOF biped robot, IEEE Trans. on Robotics and Automation, 19 (4), 653-668 (2003).

[4] K. Mombaur, Using optimization to create self-stable human-like running, Robotica, 27 (03), 321-330 (2009).

[5] L. Roussel and C. Canudas-De-Wit, Generation of energy optimal complete gait cycles for biped robots, Proc. IEEE ICRA, 2036-2041 (1998).

[6] C. Chevallereau and A. Formalsky, Low energy cost reference trajectories for a biped robot, Proc. 1998 IEEE ICRA, 1398-1404 (1998).

[7] J. Morimoto and G. Endo, Modulation of simple sinusoidal patterns by a coupled oscillator model for biped walking, Proc. 2006 IEEE ICRA, 1579-1584 (2006).

[8] T. Reil and P. Husbands, Evolution of central pattern generators for bipedal walking in a real-time physics environment, IEEE Trans. on Evolutionary Computation, 6 (2), 159-168 (2002).

[9] Y. Hasegawa and T. Arakawa, Trajectory generation of biped locomotion robot, Mechatronics, 10, 67-89 (2000).

[10] M. Hobon, N. Lakbakbi, E. Yaaqoubi, and G. Abba, Quasi Optimal Gait of a Biped Robot with a Rolling Knee Kinematic, Preprints of the 18th IFAC World Congress Milano (Italy) August 28-September 2, 2011.

[11] J. H. Yoon, O. Kwon, J. S. Yeon, and J. H. Park, Optimal Trajectory Generation of Serially-Linked Parallel Biped Robots, Proceedings of the 2006 IEEE International Conference on Robotics and Automation Orlando, Florida - May 2006.

[12] S. Piao, Q. B. Zhong, X. F. Wang, and C. Gao, Optimal Trajectory Planning for Robot, Advanced Materials Research Volumes 255 - 260, 2091-2094 (2011).

[13] Peiman Naseradin Mousavi, C. Nataraj, Ahmad Bagheri, and Mahdi Alizadeh Entezari, Mathematical simulation of combined trajectory paths of a seven link biped robot, Journal of Applied Mathematical Modeling, Volume 32, Issue 7, 1445-1462 (2008).

[14] Peiman Naseradin Mousavi and Ahmad Bagheri, Mathematical simulation of a seven link biped robot on various surfaces and ZMP considerations, Journal of Applied Mathematical Modeling, Volume 31, Issue 1, 18-37 (2007).

[15] S. Kirkpatrick, C. D. Gelatt, and P. M. Vecchi, Optimization by simulated annealing, Science, 220(4598), 671680 (1983).

[16] V. Cerny, Thermodynamical approach to the traveling salesman problem: An efficient simulation algorithm, Journal of Optimization Theory and Applications, 45(1), January, 4151 (1985).

[17] N. Metropolis, A. W. Rosenbluth, M. N. Rosenbluth, A. H. Teller, and E. Teller, Equation of state calculations by fast computing machines, The Journal of Chemical Physics, 21(6), 10871092(1953).

Copyright © 2013 by ASME